

<https://doi.org/10.1038/s43247-024-01230-z>

A lower crust shear zone facilitates delamination and continental subduction under the Apennines

Check for updates

Irene Menichelli ^{1,2} ✉, Irene Bianchi ^{2,3} & Claudio Chiarabba ^{2,3}

Physical properties and structure of the lithosphere are the first step to constrain the evolution of mountain belts. Here we show detailed shear wave velocity profiles of the lithosphere in the Apennines that clarify a controversial aspect of continental subduction: the intricate mechanism of crust delamination from the downgoing plate. From the analysis of complete and dense teleseismic Receiver Function data set, we find that the delamination of the continental lithosphere is favored by the development of a low seismic shear wave velocity zone in the middle-lower crust. We observe a double Moho below the external portions of the present mountain range, suggesting the progressive formation of the shallow interface. The delamination edge is located in the forearc, far eastward than expected, implying that the re-equilibration of the thermal unbalance, generated by the mantle substitution, may last 10-7 Myr.

The Apennines is a post-collisional belt, characterized by a complex geological history and tectonic evolution¹⁻⁶, resulting from the convergence between the Eurasian and African plates⁷. The abundance of geologic and geophysical data candidate the belt as an open laboratory for understanding continental collision and subduction. Despite the extensive studies of past decades, lively debates on the evolution of the Apennines continuously fuel the interests on peculiar geodynamic aspects. Among them, how continental subduction develops at the margin of an oceanic subduction⁸, and which are the drivers of the continental delamination⁹⁻¹³. While seismicity¹⁴ and velocity models of the mantle¹⁵⁻¹⁷ put some first order constraints on the Apennines structure and deformation, a general consensus is still far to come for understanding the dynamics of the system shaping the belt.

Past tomographic models^{15,18-21} and other imaging techniques²²⁻³⁰ have suggested the lateral discontinuity of subduction with a slab window along the central Apennines³¹, marked by a low-velocity zone at lithospheric depth mirrored by the lack of intermediate-depth seismicity^{27,32}. Anyway, recent models proposed that the same features could be related to heterogeneities of the Adria continental lithosphere³³, which also affected the different evolution of subduction between the northern and southern portions of the chain. Previous studies have proposed that continental subduction is favored by the delamination of the lithosphere^{11,12,24,34-36} characterized by a different level of maturity along the belt. This has caused spatial and temporal heterogeneity in the evolution of the Apennines, different amount of seismicity and seismic energy released, and the partitioning of seismic versus ductile deformation from north to south of the chain³⁴. Recent studies have

revealed also how continental subduction in general is deeply related to the rheological behavior of the crust and the slab itself, and to the mechanical coupling at the Moho boundary^{10,37,38}. These physical conditions also control the process of delamination, which can take the place or delay the slab detachment^{39,40}.

In this study, we investigate how the evolution of a decoupled subduction orogen like the Apennines is entangled with the structure of the continental lithosphere that is underthrusting. We used teleseismic RF analysis to define crustal properties and bulk velocity models of the Adria lithosphere, and extract information on geometric interfaces, from harmonics analysis of the Q (i.e., radial) and the T (i.e., transversal) components²³. In the first step, we compute 1D-shear wave velocity profiles of the entire lithosphere with a trans-dimensional non-linear method⁴¹ for a dense set of seismic stations displaced along our study area (see Fig. 1). Then, we select shear wave velocity profiles representative for the different sectors of the belt (fore-arc - belt - back-arc) and compare velocity results with the crustal-mantle structure obtained by new tomographic models³⁵.

Results

Harmonic analysis

RFs data clearly show a difference in the velocity structure between the inner and outer sectors of the belt. Specifically, the results of three seismic stations (CSNT, CRE, and MPAG; orange triangles in Figs. 1 and 2) located across the chain are exemplary to summarize the lateral change of the seismic structure perpendicular to the belt strike.

¹Dipartimento di Scienze, Università degli Studi Roma Tre, Largo San Leonardo Murialdo, Rome 00146, Italy. ²Istituto Nazionale di Geofisica e Vulcanologia, Via di Vigna Murata 605, Rome 00143, Italy. ³These authors contributed equally: Irene Bianchi, Claudio Chiarabba. ✉e-mail: irene.menichelli@ingv.it

We plotted the results of the RFs analysis (Fig. 2) and the harmonic decomposition (Fig. 3) for the three harmonic orders (i.e., $k=0, 1, 2$) to show the isotropic ($k=0$) and anisotropic ($k=1, 2$) modeled and unmodeled

("Q-iT") components. Blue and red pulses indicate the positive/negative amplitudes, respectively, in the RF traces.

In addition, we show a profile across the belt of shear wave velocity and tomographic images (Fig. 4d). In the backarc region (station CSNT, Fig. 4a), the isotropic ($k=0$) component (Fig. 3) reveals a strong positive pulse at ~3.5–4.0 s, related to the conversion at the Tyrrhenian Moho, consistent with the jump in shear wave velocity observed at 25 km (Fig. 4). A similar observation can be made by looking at the isotropic component below the belt (CRE station, Fig. 3), again a positive pulse is present at around 4 s, but less sharp than that observed in the back-arc region. Nevertheless, again, the conversion can be related to the single Tyrrhenian Moho found at a depth of 27 km from the shear wave velocity profile (Fig. 4b). Below the Moho, shear wave velocities are ~4.0 km/s at upper mantle depth, values lower than those in the back-arc region (shear wave velocity ~4.3–4.5 km/s).

In the forearc (station MPAG, Fig. 4a) the shear wave velocity model shows two velocity peaks of 4.1 km/s related to different Moho depths at 27 and 52 km and is consistent with the two pulses, a weaker one at 2.5–3.0 s negative pulse and one stronger at 6 s positive pulse in the isotropic harmonic components (Fig. 4c). These two depths are likely related to the presence of a double Moho. Between these two interfaces, a strong decrease in S-wave velocity is observed, with values as small as 3.6 km/s at ~40 km, while in the uppermost mantle (below 52 km) velocity becomes stable at 4.3–4.4 km/s coherent with the Adriatic LID (LID= lithosphere)^{12,42,43}.

Profile A-A' (see Fig. 4) shows the main differences in the velocity structure and Moho depth between the Tyrrhenian and Adriatic coasts, pointing out the location of a probable suture zone between the two domains. Below the OSSC, CSNT and CRE stations (Fig. 4a) the strong

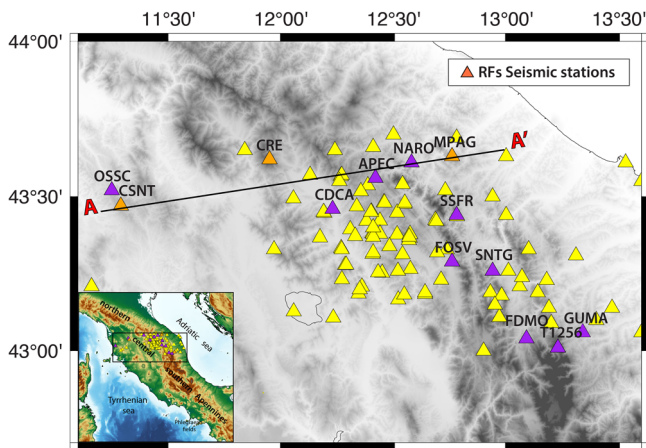


Fig. 1 | Map showing the seismic stations (triangles) used for the Receiver Function analysis. Orange triangles indicate stations whose analysis results are reported in Figures 2, 3. The shear wave velocity profiles of the seismic stations (purple) crossed by the traces (black lines) are reported in Fig. 4 and in the SI. The yellow triangles represent all the other stations analyzed (reported in SI).

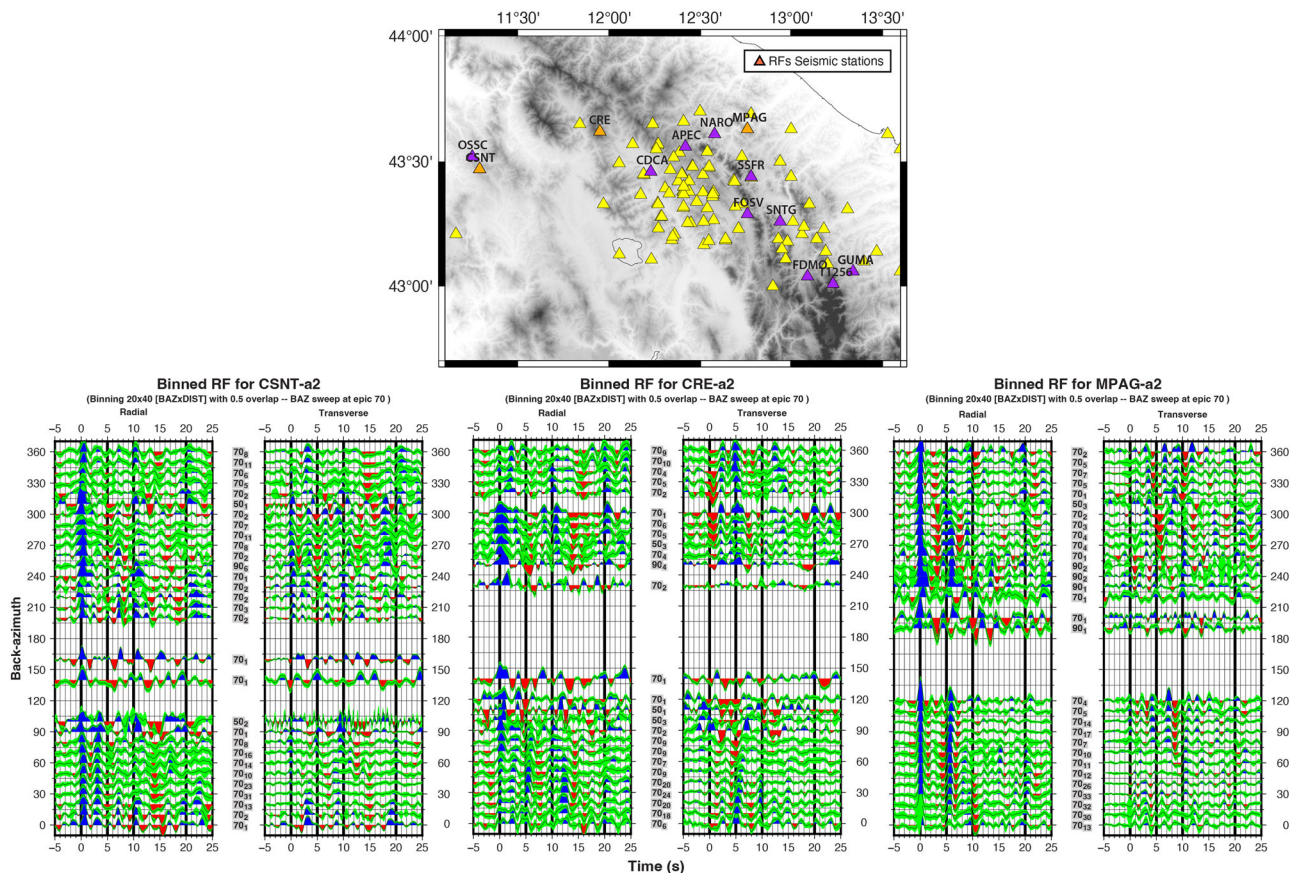


Fig. 2 | Representative analyzed Receiver Functions. On top, purple triangles indicate the location of the seismic stations analyzed. Whereas, in orange three representative seismic stations, CSNT, CRE and MPAG, which results are reported in the three bottom panels. On bottom, the analyzed Receiver Functions are reported for back-azimuth values and epicentral distance (i.e., numbers highlighted in gray).

Blue and red wiggles show positive and negative amplitudes in the RF, respectively. Green shading shows variance of the individual bin-averaged RFs. Our method is based on the extraction of the back-azimuth harmonics from the RFs data set as a function of the incoming P-wavefield direction.

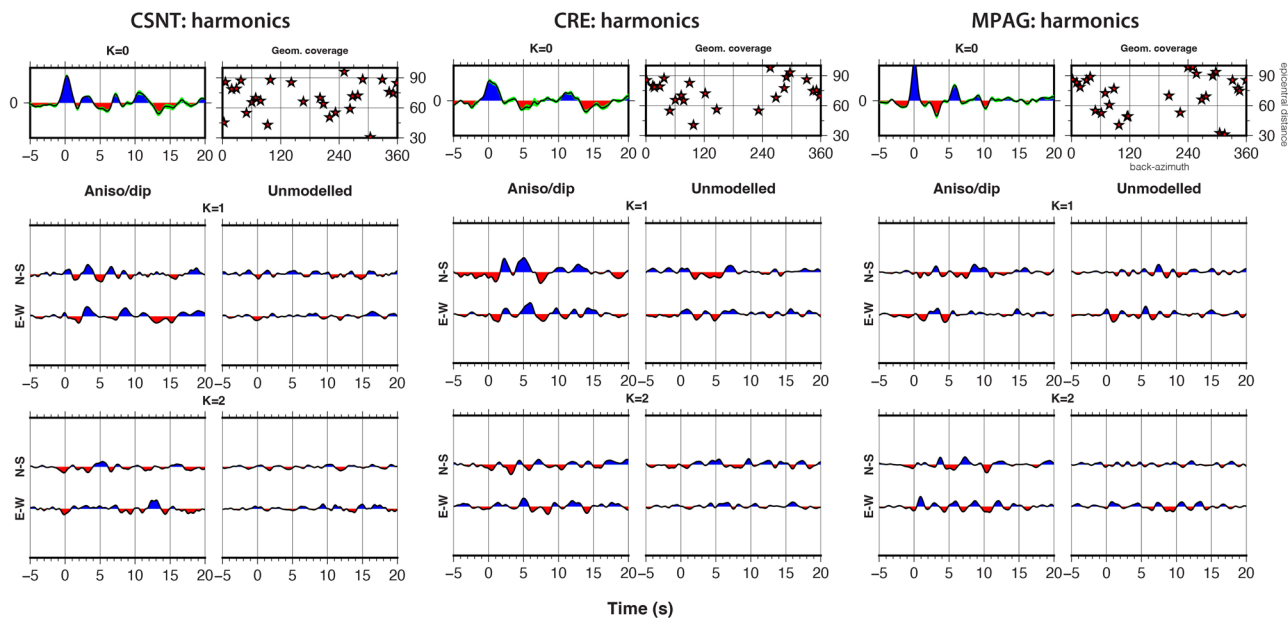


Fig. 3 | Harmonic decomposition for CSNT, CRE and MPAG stations (see Fig. 1). On top panels the isotropic component (i.e., $k=0$) (left) and the geometric coverage (right). On the center and bottom left panels the anisotropic components for the first and second harmonic ($k=1$ and 2) orders are shown. On the right the unmodelled components (“Q-IT”) are reported.

velocity jump marks the Moho depth ~ 25 – 27 km, consistent with earlier studies^{44–46} and with the crustal extension and shallower Moho due to the opening of the Tyrrhenian basin. The distribution of shear wave velocity below the CDCA seismic station appears very interesting, as compared to the other profiles. It is not characterized by a strong increase in velocities (~ 4.1 km/s), probably due to the fact that the station is located above the suture zone between the Adriatic and Tyrrhenian coasts. Moving toward the east, the velocity distribution below the seismic stations located in the inner portion of the belt (CDCA and APEC) results to be smoother, with the absence of a strong jump marking the Tyrrhenian Moho depth. Below APEC, at a depth of around 45–50 km, a smooth increase of about 1 km/s is depicted, and also below the CDCA, at 74 km, there is a gentle jump; these may be related to the deeper Adriatic Moho plunging westward. In the end, the velocity structure below NARO and MPAG is characterized by two sharp jumps at around 26–27 km and 52–54 km depth, respectively, that could be associated with the presence of a double Moho: the deeper Adriatic one and the incipient Tyrrhenian Moho. These results highlight the different velocity structure that distinguishes the Adriatic from the Tyrrhenian domain, where a thinner crust predominates in the latter, while the Adriatic crust is apparently thicker in agreement with⁴². Hence, the analysis of the velocity profiles and the isotropic component of the RFs suggests three main different zones with peculiar crustal thickness, Moho depth and velocity interfaces.

Figure 4d shows the good correspondence between the shear wave velocity jumps, extracted from the 1D velocity profiles, associated with the Adriatic (yellow crosses) and Tyrrhenian Moho (green crosses) depths, and the location of the Vp anomalies (reported in both absolute and perturbation Vp values). The Tyrrhenian Moho under the western side of the Apennines follows the transition between the low (~ 6.5 km/s) and the high Vp velocity anomaly (~ 7 – 7.5 km/s). Looking at the velocity structure below the Adriatic side, the Tyrrhenian Moho falls along the narrow horizontal anomaly defined by an increase in P-wave velocity (~ 7.5 km/s). Below that, a decrease in P-waves velocity (about 6 km/s) characterizes the depth interval between 30–38 km, followed by an increase to 7.5 km/s up to 50–55 km depth. At this depth, the Adriatic Moho is reported and seems to follow the abrupt change from 7.5 to 8 km/s. It is interesting to note how the two Moho interfaces seem to confine the broad low Vp volume (Fig. 4d, Vp pert (%)

cross-section) and its location well fits with also the decreasing in shear wave velocity below the NARO and MPAG seismic stations.

Summarizing, the basic feature that we observe is the couple of negative and positive shear wave velocity at about 25 and between 26 and 50 km depth that reverses from the back-arc to the fore-arc domains, while the internal sector has intermediate velocities.

Discussion

The harmonic analysis and inversion of RF data yield high-resolution imaging of the shear wave velocity structure of the lithosphere down to 100 km depth on a key transect across the Apennines belt. Usually, RF profiles show migrated sections of discontinuities beneath the target. Here, we present a full 1D shear wave velocity reconstruction of the lithosphere, with absolute velocities that more tightly constrain the nature of discontinuities and layers. Shear wave velocity jumps to values higher than 4.0 km/s revealed a Moho doubling for almost the entire section of the belt, suggesting that the delamination hinge of the Adria lithosphere is located further eastward in the forearc. We identify a low shear wave velocity layer (3.5–4.0 km/s) between 25 and 54 km depth below the forearc that indicates the presence of a slow lower crust, in correspondence with a tomographic low Vp volume where intermediate seismicity develops. Part of this low-Vp volume is coupled with high Vp/Vs suggesting the presence of fluids, consistent with the shear wave velocity reduction. All these elements support the scenario in which a shear zone develops within a weak lower crust along which the continental delamination of the Adria lithosphere takes place. We propose that the weakness of the lower crust is the main factor that controls the delamination of the lithosphere, in agreement with numerical models where the coupling between the crust and subducting lithosphere is governed by the rheology^{40,47}.

In the forearc, the doubled pulse of positive RF suggests that the newly formed Moho is under development. Interestingly, the negative pulses at around 3–4s detected under the stations in this Apennine sector (NARO and MPAG, Fig. 4c) are related to the negative jump in the related shear wave velocity models (Fig. 4b) indicating a velocity reversal within the Adria lower crust, signature of the ongoing delamination and immature re-formation of the Moho. The replacement of sublithospheric mantle after delamination generates a thermal unbalance beneath the mountain range. This causes the

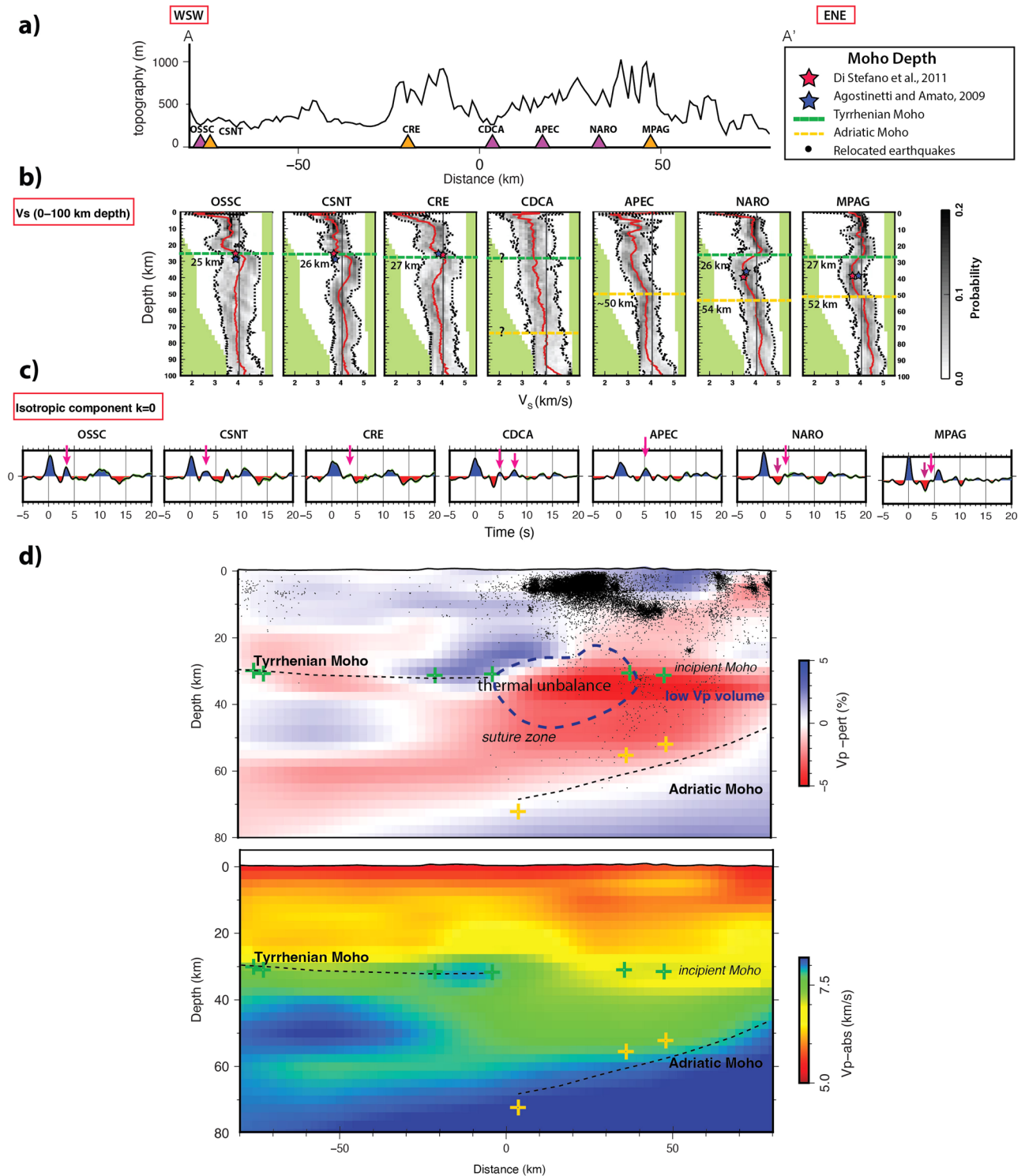


Fig. 4 | Comparison of the velocity structure between the western and eastern side of the north-central Apennines. **a** Topography of the profile A–A' in the map (see Fig. 1) with the location of the seismic stations reported below. **b** 1D shear wave velocity model (0–100 km depth) for the seismic stations crossed by the trace. The red line indicates the average S-wave velocity, while the standard deviation interval falls within the black lines. Yellow and green dashed lines define the Adriatic and Tyrrhenian Moho depth, respectively. The red and blue stars are the Moho depth extracted from⁴⁵ and⁴⁴. The green color is the background color. **c** Isotropic

composition ($k=0$) along time (s) extracted by the Rf's analysis at the different seismic stations. Blue and red lobes indicate positive and negative pulses. The light pink arrows indicate pulses related to mature Moho, the dark ones to non-mature Moho. **d** The corresponding 3D V_p cross-sections from the model of⁶⁵. The black dots are relocated earthquakes (2005–2020) in the 1D velocity models of the Central Mediterranean computed in the work of Menichelli et al., 2022. The green and yellow crosses represent the Tyrrhenian and Adriatic Moho depths extracted from the shear wave velocity 1D models for each seismic station, respectively.

intense stretching, extensional deformation, and partial melting of the crust leading to plutonism, and magmatic activity.

In the back arc region (section d, Fig. 4), a low shear wave velocity ($V_s = 3.3\text{--}3.8$ km/s) is observed in the lower crust, consistent with partial melting due to the high temperature at the base of the crust. At mantle depth, we observe a normal shear wave velocity and slight low Vp at 30 km depth, rapidly becoming high Vp at greater depths, indicating that the mantle top is mostly re-normalized after the first episode of delamination in the Apennines (fossil delamination event), where associated plutonism and stretching date back of around 10–7 Myr^{48,49}. Therefore, on this side of the chain, the thermal re-equilibration process is mature, in contrast to the forearc zone where the low shear wave velocity and low Vp anomalies predominate. The strong anisotropy observed in the k1 components at stations in the backarc (Fig. 3) is consistent with a deeply hydrated mantle^{42,50,51}. The crust characterized by weak rheology (e.g., wet quartzite) resists subduction, inhibiting detachment but leading to its extrusion and delamination. In that case, the low Vp and Vp/Vs can be due to a crust composed by granitic rocks that have taken place of a mafic mid-lower crust during the process of delamination⁵². Consequently, the crustal-lithospheric structure of the belt is characterized by a buckling crust uncoupled from the slab, features that are reflected as the chain broadens at the surface⁴⁰. The case of the northern Apennines turns out to be the example that best fits a decoupled orogenic system⁴⁷ characterized by the development of a low-shear wave zone in a weak mid-lower crust zone.

In our proposed model, the weak lower crust inhibits the detachment of the continental slab, promoting a prolonged process of delamination, subduction and retreat of part of the lower crust remaining attached to the mantle lithosphere of Adria. Fluids liberated from the eclogitization of the lower crust promotes further delamination and retreat of the lithosphere. The incipient formation of the double Moho observed beneath the forearc has a mature-stage analog in the backarc, where crustal thinning and magmatism followed the reformation of the shallow Tyrrhenian Moho. This hypothesis leads to the definition of a new scenario for the Apennine subduction where the starting point of delamination is in the forearc and a longer thermal rebalancing is required. This suggests that a continental subduction can be sustained over time if it develops at mid-lower crustal depths within weak rheology inhibiting the slab break-off process. Our results offer a new vision of continental subduction and a prognostic long-term indication for the evolution of the Apennines in the next 7–10 Myr.

Online method

The Teleseismic Receiver Function analysis is one of the most suitable techniques for identifying velocity boundaries such as Moho or LAB^{23,53,54} and reconstructing local crust-mantle geometry. Receiver functions are time series that isolate the converted P-to-S phases within the coda of the teleseismic waves. A deconvolution process is applied to separate the vertical component from the horizontal one⁵⁵.

In this work, we analyzed RFs (i.e., teleseismic receiver functions) recorded by seismic stations, deployed along the north-central Apennines, in order to define the S-wave velocity structure for the entire lithosphere (up to 100 km depth), revealing the lateral and vertical heterogeneities and the Moho depth. A detailed comparison between the results of the west- and east-ward seismic stations is reported to highlight the main structural differences between the inner and outer section of the chain. In the end, the shear wave velocity profile computed has been directly compared with a new regional tomographic model³⁵. Our dataset was made by 15,000 RFs derived from teleseismic events at epicentral distances between 30° and 100°, and with $M_w \geq 5.5$, selected by their high signal-to-noise ratio. Teleseismic events were recorded between 2012–2020 by 56 broad-band (RSN), three-component stations, located in the north-central Apennines, between 43° N – 43.7° N and 10.6° E – 13.3° E (Fig. 1). The seismic records have been rotated to analyze the Ps converted phase in the LQT reference system, where L is the direction of the theoretical direction of the incoming P wave, whereas Q is perpendicular to L in the plane that contains the source and the receiver (i.e., vertical plane).

We filtered the teleseismic waves with a pass frequency cutoff of 5–0.02 Hz, implying a wavelength in the mantle between 1.6 – 400 km. In the past, the effect of different high-frequency (0.5 – 1–2– 4 Hz) filters on the uncertainties has been tested (Agostinetti and Malinverno, 2018) showing the reliability of the multifrequency RF inversion results. In the past, the effect of different frequency (0.5 – 1–2– 4 Hz) filters on the uncertainties has been tested (Agostinetti and Malinverno, 2018) showing the reliability of the multifrequency RF inversion results. In particular, the average resolution of 1D shear wave velocity profiles is around 10% of the depth of the discontinuity. Furthermore, the shear wave velocity uncertainties result small for a data set acquired for a minimum period of 3–12 months discarding the possibility to insert artifacts in the computed posterior velocity distribution. We followed a technique developed by^{53,56} to compute receiver functions from multitaper correlation estimates by a frequency domain algorithm.

For each seismic station analyzed, we obtained the Q-RFs (radial) and the T-RFs (transversal) (Fig. 2) and used the Q-RFs to retrieve the shear wave velocity models up to 100 km depth (Fig. 4 and SI). Our analysis is based on the extraction of the back-azimuth harmonics from the RFs as a function of the incoming P-wavefield direction (Bianchi et al., 2010a). Thanks to this decomposition technique, it is possible to derive information on the periodicity of the signal. The analysis was made on the first three degrees and orders, $k = 0, 1, 2$ (see Fig. 2). Despite that, we mainly focused on the results of the $k = 0$ component, corresponding to the constant back-azimuth harmonic and representing the isotropic structure below the seismic station.

Harmonic Analysis

We follow the method described in detail by⁵⁶ based on the harmonics decomposition of the RF signal, and to which we refer for deeper insights. The technique permits to compute both the Q and T components and it has been applied in previous works^{22,23,44,57} to investigate the velocity structures of several geodynamic settings such as subduction zones or volcanic areas. In this study, we obtained the $k = 0$ back-azimuth harmonic of the Q-RF data set through a simple stack of the Q-RF components over back-azimuth values. Meanwhile, the energy reflected by dipping interfaces or anisotropic layers have been recorded on the first ($k = 1$) and second ($k = 2$) harmonics, displaying a periodicity of respectively $2\pi/k$ and π/k with the incoming P-wave back azimuth. In particular, the two or four lobes periodicity, can be associated respectively to a plunging symmetry axis at depth or an anisotropic layer with horizontal symmetry axis⁵⁸.

Figure 3 shows the results of the decomposition of the Q and T components for three reference seismic stations reported in map (orange triangles in Fig. 1). The traces with $k = 0$ show the isotropic component constant with the back azimuth, whereas for the components of higher grade also the unmodelled part (“Q-iT”) is reported displaying lower energy. The standard deviation of the bootstrapped harmonics is highlighted by green lines that envelop the traces in the graphics. To assure the analysis of good signals also the analysis of the geometric coverage for each seismic station have been done and reported.

Shear wave velocity inversions

The RF inversion problem can lead to several solutions, among them the best-fit velocity model or the probability distribution of velocity parameters along the depth. The non-uniqueness of the problem means that it is not possible to find a single solution⁵⁹. For that reason, several inversion techniques have been developed with the aim to overcome and manage this problem. Among them⁴¹, adopt a Reversible-jump Markov chain Monte Carlo (RjMCMC) scheme to compute a 1D shear wave velocity model, solving the nonlinear inverse problem, for each seismic station. The advantage of this approach lies in the limited dependence of the final solution on a-priori information; even S-wave velocities and the number of layers are treated as unknown. Hence, at the end of the procedure, the posteriori probability distribution (PPD) of inverted parameters indicates how many seismic interfaces are located below each station and their most probable depth. The $k = 0$ harmonics and their standard deviations are used

to define the isotropic structure of the lithosphere calculating the posterior probability distribution.

This technique is based on the searching into a multidimensional parameter space exploiting the Voronoi cells properties to find, not the best fit model but a distribution of models with an acceptable data fit. During an initial burn-in phase, 100,000 models were discarded from a total of 200,000 random models calculated for each of the 100 RjMcMc parallel independent Markov chains. Hence, the RjMcMc search was run and the posterior probability density function (PPD) was obtained using the remaining velocity models (for an ensemble of 10^7 models). Finally, the output of this inversion procedure are the PPD of the Vs and Vp/Vs (Figs. 4b and SI), the mean model and the distribution of the interfaces up to 100 km depth.

Data availability

Earthquake and waveform data of Italian seismicity have been provided by Istituto Nazionale di Geofisica e Vulcanologia (INGV) and can be retrieved in the EIDA database (<http://eida.rm.ingv.it>).

Code availability

The original source code to compute the shear wave velocity model was obtained from Agostinetti and Malinverno (2010).

Received: 12 September 2023; Accepted: 19 January 2024;

Published online: 19 February 2024

References

- Dogliani, C. A proposal for the kinematic modelling of w-dipping subductions—possible applications to the tyrrhenian-apennines system. *Terra Nova* **3**, 423–434 (1991).
- Dogliani, C., Carminati, E., Cuffaro, M. & Scrocca, D. Subduction kinematics and dynamic constraints. *Earth-Sci. Rev.* **83**, 125–175 (2007).
- Malinverno, A. & Ryan, W. B. Extension in the tyrrhenian sea and shortening in the apennines as result of arc migration driven by sinking of the lithosphere. *Tectonics* **5**, 227–245 (1986).
- Carminati, E., Lustrino, M., Cuffaro, M. & Dogliani, C. et al. Tectonics, magmatism and geodynamics of italy: what we know and what we imagine. *J. Virtual Expl.* **36**, 10–3809 (2010).
- Carminati, E. & Dogliani, C. Alps vs. apennines: The paradigm of a tectonically asymmetric earth. *Earth-Sci. Rev.* **112**, 67–96 (2012).
- Faccenna, C., Becker, T. W., Miller, M. S., Serpelloni, E. & Willett, S. D. Isostasy, dynamic topography, and the elevation of the apennines of italy. *Earth Planet Sci. Lett.* **407**, 163–174 (2014).
- Dewey, J., Helman, M., Knott, S., Turco, E. & Hutton, D. Kinematics of the western mediterranean. *Geol. Society London, Special Publicat* **45**, 265–283 (1989).
- Faccenna, C., Becker, T. W., Lucente, F. P., Jolivet, L. & Rossetti, F. History of subduction and back arc extension in the central mediterranean. *Geophys. J. Int.* **145**, 809–820 (2001).
- Göğüş, O. H. & Pysklywec, R. N. Near-surface diagnostics of dripping or delaminating lithosphere. *J. Geophys. Res. Solid Earth* **113** (2008).
- Faccenda, M., Gerya, T. V. & Burlini, L. Deep slab hydration induced by bending-related variations in tectonic pressure. *Nat. Geosci.* **2**, 790–793 (2009).
- Chiarabba, C., Giacomuzzi, G., Bianchi, I., Agostinetti, N. P. & Park, J. From underplating to delamination-retreat in the northern apennines. *Earth Planetary Sci. Lett.* **403**, 108–116 (2014).
- Chiarabba, C., Buttinelli, M., Cattaneo, M. & De Gori, P. Large earthquakes driven by fluid overpressure: The apennines normal faulting system case. *Tectonics* **39**, e2019TC006014 (2020).
- D'Acquisto, M. et al. Tectonics and seismicity in the northern apennines driven by slab retreat and lithospheric delamination. *Tectonophysics* **789**, 228481 (2020).
- Chiarabba, C., De Gori, P. & Mele, F. M. Recent seismicity of italy: Active tectonics of the central mediterranean region and seismicity rate changes after the mw 6.3 l'aquila earthquake. *Tectonophysics* **638**, 82–93 (2015).
- Piromallo, C. & Morelli, A. P wave tomography of the mantle under the Alpine-Mediterranean area. *J. Geophys. Res. Solid Earth* **108**, 1–23 (2003).
- Di Stefano, R., Kissling, E., Chiarabba, C., Amato, A. & Giardini, D. Shallow subduction beneath Italy: Three-dimensional images of the Adriatic-European-Tyrrhenian lithosphere system based on high-quality P wave arrival times. *J. Geophys. Res. Solid Earth* **114**, 1–17 (2009).
- Giacomuzzi, G., Chiarabba, C. & De Gori, P. Linking the alps and apennines subduction systems: new constraints revealed by high-resolution teleseismic tomography. *Earth Planetary Sci. Lett.* **301**, 531–543 (2011).
- Lucente, F. P., Chiarabba, C., Cimini, G. B. & Giardini, D. Tomographic constraints on the geodynamic evolution of the italian region. *J. Geophys. Res. Solid Earth* **104**, 20307–20327 (1999).
- Wortel, M. & Spakman, W. Subduction and slab detachment in the mediterranean-carpethian region. *Science* **290**, 1910–1917 (2000).
- Rosenbaum, G., Gasparon, M., Lucente, F. P., Peccerillo, A. & Miller, M. S. Kinematics of slab tear faults during subduction segmentation and implications for italian magmatism. *Tectonics* **27** (2008).
- Giacomuzzi, G., Civalleri, M., De Gori, P. & Chiarabba, C. A 3d vs model of the upper mantle beneath italy: Insight on the geodynamics of central mediterranean. *Earth Planetary Sci. Lett.* **335**, 105–120 (2012).
- Mele, G., Sandvol, E. & Cavinato, G. P. Evidence of crustal thickening beneath the central apennines (italy) from teleseismic receiver functions. *Earth Planet Sci. Lett.* **249**, 425–435 (2006).
- Bianchi, I., Park, J., Piana Agostinetti, N. & Levin, V. Mapping seismic anisotropy using harmonic decomposition of receiver functions: An application to northern apennines, italy. *J. Geophys. Res. Solid Earth* **115** (2010).
- Miller, M. S. & Piana Agostinetti, N. Insights into the evolution of the italian lithospheric structure from s receiver function analysis. *Earth Planet. Sci. Lett.* **345–348**, 49–59 (2012).
- Sun, D., Miller, M. S., Agostinetti, N. P., Asimow, P. D. & Li, D. High frequency seismic waves and slab structures beneath italy. *Earth Planet. Sci. Lett.* **391**, 212–223 (2014).
- Salimbeni, S. et al. Seismic anisotropy across adria plate, from the apennines to the dinarides. *Front Earth Sci.* **10**, 881138 (2022).
- Amato, A., Alessandrini, B., Cimini, G., Frepoli, A. & Selvaggi, G. Active and remnant subducted slabs beneath italy: evidence from seismic tomography and seismicity (1993).
- Spakman, W. & Wortel, R. A tomographic view on western mediterranean geodynamics. In *The TRANSMED Atlas. The Mediterranean region from crust to mantle: Geological and geophysical framework of the Mediterranean and the surrounding areas*, 31–52 (Springer, 2004).
- Zhao, L. et al. Continuity of the alpine slab unraveled by high-resolution p wave tomography. *J. Geophys. Res. Solid Earth* **121**, 8720–8737 (2016).
- El-Sharkawy, A. et al. The slab puzzle of the alpine-mediterranean region: Insights from a new, high-resolution, shear wave velocity model of the upper mantle. *Geochem. Geophys. Geosyst.* **21**, e2020GC008993 (2020).
- Rosenbaum, G. & Piana Agostinetti, N. Crustal and upper mantle responses to lithospheric segmentation in the northern apennines. *Tectonics* **34**, 648–661 (2015).
- Chiarabba, C., Jovane, L. & DiStefano, R. A new view of italian seismicity using 20 years of instrumental recordings. *Tectonophysics* **395**, 251–268 (2005).
- Giacomuzzi, G., De Gori, P. & Chiarabba, C. How mantle heterogeneities drive continental subduction and magmatism in the apennines. *Sci. Rep.* **12**, 13631 (2022).

34. Chiarabba, C., Menichelli, I., Bianchi, I., Giacomuzzi, G. & De Gori, P. Continental subduction of adria in the apennines and relation with seismicity. *Front. Earth Sci.* **11**, 1253443.
35. Menichelli, I., De Gori, P., Lucente, F. P., Improta, L. & Chiarabba, C. Lithosphere structure, processes, and physical state of the alpine-apennine system. *J. Geophys. Res. Solid Earth* **128**, e2023JB026411 (2023).
36. Latorre, D., Di Stefano, R., Castello, B., Michele, M. & Chiaraluce, L. An updated view of the italian seismicity from probabilistic location in 3d velocity models: The 1981–2018 italian catalog of absolute earthquake locations (class). *Tectonophysics* **846**, 229664 (2023).
37. Andrews, E. R. & Billen, M. I. Rheologic controls on the dynamics of slab detachment. *Tectonophysics* **464**, 60–69 (2009).
38. Schmalholz, S. M. A simple analytical solution for slab detachment. *Earth Planet. Sci. Lett.* **304**, 45–54 (2011).
39. Bird, P. Continental delamination and the colorado plateau. *J. Geophys. Res. Solid Earth* **84**, 7561–7571 (1979).
40. Duretz, T. & Gerya, T. Slab detachment during continental collision: Influence of crustal rheology and interaction with lithospheric delamination. *Tectonophysics* **602**, 124–140 (2013).
41. Agostinetti, N. P. & Malinverno, A. Receiver function inversion by trans-dimensional monte carlo sampling. *Geophys. J. Int.* **181**, 858–872 (2010).
42. Agostinetti, N. P., Bianchi, I., Amato, A. & Chiarabba, C. Fluid migration in continental subduction: The northern apennines case study. *Earth Planet. Sci. Lett.* **302**, 267–278 (2011).
43. Piana Agostinetti, N., Giacomuzzi, G. & Malinverno, A. Local three-dimensional earthquake tomography by trans-dimensional monte carlo sampling. *Geophys. J. Int.* **201**, 1598–1617 (2015).
44. Piana Agostinetti, N. & Amato, A. Moho depth and vp/vs ratio in peninsular italy from teleseismic receiver functions. *J. Geophys. Res. Solid Earth* **114** (2009).
45. Di Stefano, R., Bianchi, I., Ciaccio, M. G., Carrara, G. & Kissling, E. Three-dimensional moho topography in italy: New constraints from receiver functions and controlled source seismology. *Geochem. Geophys. Geosyst.* **12** (2011).
46. Spada, M., Bianchi, I., Kissling, E., Agostinetti, N. P. & Wiemer, S. Combining controlled-source seismology and receiver function information to derive 3-D moho topography for italy. *Geophys. J. Int.* **194**, 1050–1068 (2013).
47. Faccenda, M., Gerya, T. V. & Chakraborty, S. Styles of post-subduction collisional orogeny: Influence of convergence velocity, crustal rheology and radiogenic heat production. *Lithos* **103**, 257–287 (2008).
48. Jolivet, L. et al. Interactions of plutons and detachments: a comparison of aegean and tyrrhenian granitoids. *Solid Earth* **12**, 1357–1388 (2021).
49. Avanzinelli, R., Lustrino, M., Mattei, M., Melluso, L. & Conticelli, S. Potassic and ultrapotassic magmatism in the circum-tyrrhenian region: significance of carbonated pelitic vs. pelitic sediment recycling at destructive plate margins. *Lithos* **113**, 213–227 (2009).
50. Agostinetti, N. P. & Miller, M. S. The fate of the downgoing oceanic plate: Insight from the northern cascadia subduction zone. *Earth Planet. Sci. Lett.* **408**, 237–251 (2014).
51. Audet, P. Layered crustal anisotropy around the san andreas fault near parkfield, california. *J. Geophys. Res. Solid Earth* **120**, 3527–3543 (2015).
52. Guo, Z. et al. High resolution 3-d crustal structure beneath ne china from joint inversion of ambient noise and receiver functions using necessarray data. *Earth Planet. Sci. Lett.* **416**, 1–11 (2015).
53. Park, J. & Levin, V. Receiver functions from multiple-taper spectral correlation estimates. *Bull. Seismol. Society America* **90**, 1507–1520 (2000).
54. Miller, M. S. & Piana Agostinetti, N. Erosion of the continental lithosphere at the cusps of the calabrian arc: Evidence from s receiver functions analysis. *Geophys. Res. Lett.* **38** (2011).
55. Langston, C. A. Structure under mount rainier, washington, inferred from teleseismic body waves. *J. Geophys. Res. Solid Earth* **84**, 4749–4762 (1979).
56. Park, J. & Levin, V. Anisotropic shear zones revealed by backazimuthal harmonics of teleseismic receiver functions. *Geophys. Suppl. Monthly Notices Royal Astronomical Society* **207**, 1216–1243 (2016).
57. Piana Agostinetti, N., Lucente, F., Selvaggi, G. & Di Bona, M. Crustal structure and moho geometry beneath the northern apennines (italy). *Geophys. Res. Lett.* **29**, 60–1 (2002).
58. Maupin, V., Park, J., Romanowicz, B. & Dziewonski, A. Theory and observations- "wave propagation in anisotropic media. *Seismol. Struct. Earth. Treatise Geophys.* **1**, 289–321 (2007).
59. Ammon, C. J., Randall, G. E. & Zandt, G. On the nonuniqueness of receiver function inversions. *J. Geophys. Res. Solid Earth* **95**, 15303–15318 (1990).
60. Wessel, P., Smith, W. H., Scharroo, R., Luis, J. & Wobbe, F. Generic mapping tools: improved version released. *Eos, Transact American Geophys. Union* **94**, 409–410 (2013).

Acknowledgements

Figures were made using Generic Mapping Tools (GMT) software⁶⁰. I would like to thank Andrea Licciardi for giving us valuable suggestions on data interpretation and for sharing his RFs dataset with us and Nicola Piana Agostinetti for the help in the computation of the RFs dataset.

Author contributions

Irene M. and Irene B. analyzed the teleseismic data, computed Receiver Functions data set and inverted it to obtain the shear wave velocity profiles. Irene M. and Claudio C. interpreted the results and with Irene B. wrote the text.

Competing interests

The authors declare no competing interests.

Additional information

Supplementary information The online version contains supplementary material available at <https://doi.org/10.1038/s43247-024-01230-z>.

Correspondence and requests for materials should be addressed to Irene Menichelli.

Peer review information *Communications Earth & Environment* thanks Amr El-Sharkawy, Maria Sachpazi and the other, anonymous, reviewer(s) for their contribution to the peer review of this work. Primary Handling Editors: Kim Welford and Joe Aslin. A peer review file is available.

Reprints and permissions information is available at <http://www.nature.com/reprints>

Publisher's note Springer Nature remains neutral with regard to jurisdictional claims in published maps and institutional affiliations.

Open Access This article is licensed under a Creative Commons Attribution 4.0 International License, which permits use, sharing, adaptation, distribution and reproduction in any medium or format, as long as you give appropriate credit to the original author(s) and the source, provide a link to the Creative Commons licence, and indicate if changes were made. The images or other third party material in this article are included in the article's Creative Commons licence, unless indicated otherwise in a credit line to the material. If material is not included in the article's Creative Commons licence and your intended use is not permitted by statutory regulation or exceeds the permitted use, you will need to obtain permission directly from the copyright holder. To view a copy of this licence, visit <http://creativecommons.org/licenses/by/4.0/>.

© The Author(s) 2024